Petrography and diagenetic evolution of the Barail sandstones of Naga Schuppen belt, North East India: implication towards reservoir quality

Pradip Borgohain[1], Devojit Bezbaruah[2], Manash Pratim Gogoi[1,*], Yadav Krishna Gogoi[1], Parakh Protim Phukan[2] and Deepsikha Bhuyan[2]

[1]Department of Petroleum Technology, and
[2]Department of Applied Geology, Dibrugarh University, Dibrugarh 786 004, India

Rock-thin section, scanning electron microscopy and X-ray diffraction analyses have been employed to describe in detail the mineralogical constituents, diagenetic alterations and their impact on reservoir quality of Oligocene Barail sandstones of Naga Schuppen belt, North East India. The Barail Group comprises of alternate beds of hard and compact sandstones with siltstone, shale, carbonaceous shale, and a few thin intermittent coal seams in the upper part of the rock sequence. Petrographic analysis indicates that quartz (42.02–55.02%) is the most dominant mineral constituent followed by rock fragments (6.85–15.67%) and feldspars (0.00–1.97%) with different types of cement in the studied sandstones. Quartz overgrowth, formation of pseudo matrix, authigenic growth of secondary minerals and precipitation of clay within the pore spaces tend to reduce the primary and secondary porosities of the rocks. However, in certain samples, the grain coating restricts or hinders cementation and preserves porosity during deep burial, but decreases permeability at pore throats. Partial dissolution and intragranular fracturing of the framework minerals provide sites for pore growth. Pyrite framboids and iron oxides inhibit quartz cementation, but infill pore spaces. The present study shows that original pore morphologies, as well as secondary porosities within the sandstones tend to be destroyed to a large extent by the diagenetic processes.

Keywords: Diagenetic evolution, petrography, reservoir quality, rock sequence, sandstones.

THE Naga Schuppen belt forms a part of the Assam–Arakan Sedimentary Basin, which is a shelf–slope–basinal system (Figure 1 *a*)[1]. The Schuppen belt is known for its complex structure, tectonics and occurrence of oil and coal deposits. The first commercially discovered oilfield in India, the Digboi Oilfield, is located within this belt. Two major oil fields, namely the Kharsang and Champang have been discovered within this belt. Due to complex geologic setting and certain logistic problems, the Naga Schuppen belt is poorly explored. No systematic attempt has been made so far to interpret the reservoir properties of Barail sandstones of the Naga Schuppen belt which constitute the reservoir rocks. The present study aims to characterize the Barail reservoir sandstones with respect to their mineralogical constituents, clay mineralogy and diagenetic properties. The data, so generated, may help in the adoption of proper flooding method for enhancing productivity from the aged oilfields in the basin. The present study is confined to three geological sections of the Schuppen belt, namely (i) Sonari–Tizit–Mon, (ii) Amguri–Tuli–Merangkong and (iii) Mariani–Changki–Longkhim (Figure 1 *b*).

Oligocene Barail sandstones are mainly composed of quartz, followed by rock fragments and feldspars with different types of cement (Table 1). Most of the detrital grains are sub-angular to sub-rounded in shape and show moderate to ill-sorted texture. Quartz is the dominant mineralogical constituent in all the studied samples and consists of both monocrystalline and polycrystalline varieties. There is a strong correlation between sorting and porosity in clastic reservoir sandstones. Better the sorting, higher is the porosity and permeability. The present petrographic study shows that the sandstones of bottom and middle part of the Barail Group show well-sorted texture. They consist of dominantly quartz framework grains with close packing texture. Therefore, they preserve higher porosities during burial than poorly sorted sediments. The sandstone of upper part of the Barail Group shows poorly sorted texture having more argillaceous matrix and exhibits lower porosity than sandstones of the middle and bottom parts of the Group (Table 2). Coal seams and carbonaceous shales observed during field mapping in the upper part of the Group, suggest that these sediments were deposited in a lower delta plain environment. In such depositional setting, the sediments are influenced by tides as well as fluvial activities, and as a result they exhibit poorly sorted texture. Quartz overgrowths are commonly recorded in the studied sandstones (Figure 2 *a*). The pressure solution, which is the result of compaction of sandstones, is the most important indigenous source of silica which can easily percolate through the pore spaces of coarse-grained clean sandstones and precipitate silica over the detrital quartz grains as overgrowths[2]. These quartz overgrowths deteriorate the reservoir quality of the sandstones. The study shows that the detrital rock fragments are normally weathered and show irregular grain boundaries. They consist of metamorphic rock types such as schist and gneiss detritus with prominent grain boundaries. The shale clasts and low-grade metamorphic rock fragments are converted to pseudo matrix due to deformation, which reduces the porosity and permeability of the rocks (Figure 2 *b* and *c*). Occurrence of feldspars within the studied sandstones is negligible and in many thin sections of rocks; they are completely absent. Feldspars are more susceptible to mechanical and chemical weathering, and they gradually alter to clay minerals[3]. This alteration causes cloudiness on the grains, and affects the porosity

*For correspondence. (e-mail: ta_manashgogoi@dibru.ac.in)

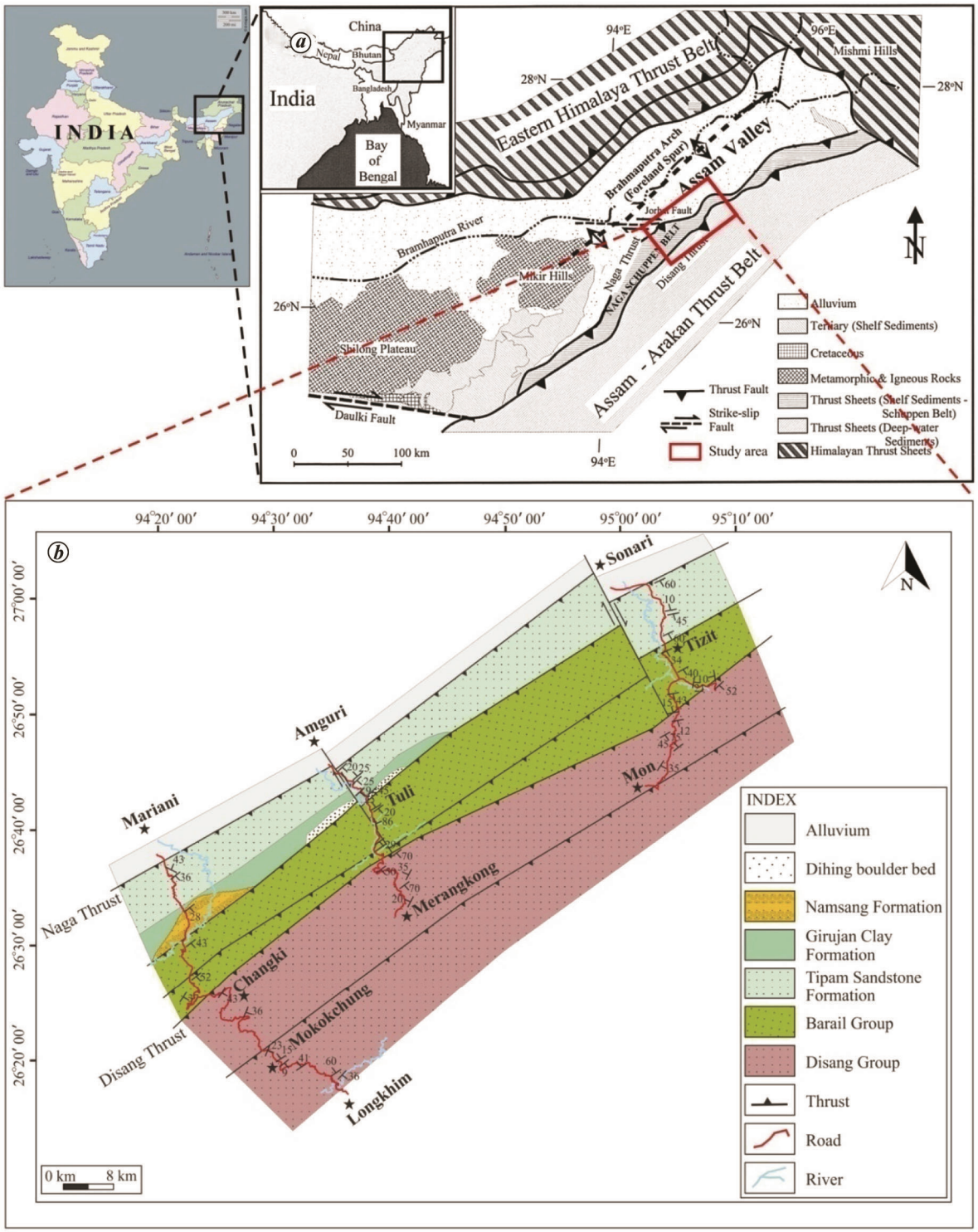

Figure 1. ***a***, Map showing Naga Schuppen belt and adjoining Upper Assam petroliferous basin (modified after Kent *et al.*[1]). ***b***, Geological map of the three studied sections.

and permeability of the rocks. Biotite is found extensively altered to chlorite; muscovite is ductile and commonly indented or deformed around the framework grains (Figure 2 *d*). The micas are relatively small in size than the constituent framework grains and they are more in fine-grained sandstones. Iron oxide cement is observed scattered within the pore spaces (Figure 2 *e*). It is also recorded as dark black coatings on the detrital quartz and feldspar grains. Occurrence of pyrite framboids suggests introduction of ferruginous solution at an early stage of diagenesis

Table 1. Percentage of framework mode of Barail sandstones

Litho-unit	Sample no.	Quartz (Q)				Quartz overgrowth (Q_O)	Feldspar (F)		Rock fragments (RF)			Cement (C)							Relative percentile %		
		Q_{Mu}	Q_{Mnu}	Q_{P2-3}	$Q_{P>3}$		F_K	$F_{Ca/Na}$	RF_{Ig}	RF_{Sed}	RF_{Met}	C_{Cal}	C_{Fe}	C_{cl}	C_{Sil}	Matrix	Mica	Chert	Q	F	RF
Upper Barail sandstones	TMK-25	15.20	18.12	2.67	7.21	2.3	0	0.78	0	5.65	8.98	0	8.63	0	8.88	16.20	3.98	4.33	73.70	1.33	24.96
	TMK-34	18.66	12.72	3.21	7.48	1.5	0	0	0	5.44	10.23	0	8.87	0	8.54	18.06	3.56	3.23	72.86	0	27.13
	TMK-36	20.34	14.61	2.89	8.06	0.00	0	0	0	4.66	8.54	0	6.34	4.29	3.53	20.02	3.37	3.35	77.66	0	22.33
	CMK-31	20.23	16.09	4.22	6.43	0.8	0	1.87	0	6.09	8.32	6.27	2.32	0	7.43	15.34	3.19	2.20	74.26	2.95	22.78
	CMK-41	18.90	18.07	3.89	4.67	0.6	0	1.98	0	4.50	8.79	0	4.12	0	10.26	18.92	3.03	2.87	74.88	3.25	21.85
	CMK-26	16.67	15.89	4.30	8.40	1.25	0	0.86	0	6.89	10.04	2.26	6.43	0	5.80	15.80	3.56	3.30	71.78	1.36	26.85
	TZM-28	20.29	14.34	3.44	11.64	2.15	0	1.64	0	5.02	7.86	3.44	4.69	0	5.21	15.55	4.23	3.40	77.39	2.55	20.05
	TZM-37	16.22	14.32	3.21	8.45	1.78	0	0.74	0	5.87	8.76	0	5.32	0	12.86	17.43	4.38	2.44	73.30	1.28	25.41
	TZM-39	17.42	16.28	4.30	6.45	0.00	0	2.14	0	7.78	6.56	0	6.23	0	10.25	15.61	3.34	3.64	72.95	3.51	23.53
Middle Barail sandstones	TMK-16	22.65	18.28	4.42	8.68	0.76	1.58	0	0	6.05	2.49	0	3.95	2.51	7.28	12.32	7.51	2.28	84.22	2.46	13.31
	TMK-18	23.58	22.21	6.20	6.79	0.00	0	0.80	0	4.46	4.20	0	6.89	0	9.06	11.42	3.19	1.20	91.78	1.24	6.96
	TMK-20	19.67	16.21	5.79	6.22	0.00	0	0	0	5.86	6.33	0	9.79	3.21	8.14	12.78	3.66	2.34	79.71	0	20.28
	TMK-21	19.42	14.58	5.32	10.29	0.43	0.79	0	0	4.21	5.43	0	7.59	2.12	8.57	12.41	4.88	4.39	82.62	1.31	16.05
	CMK-21	21.69	16.23	4.13	7.10	1.13	0.77	0	0	5.68	5.23	0	6.32	1.87	8.67	11.33	7.77	3.21	80.79	1.26	17.93
	CMK-23	18.12	16.32	5.43	10.66	0.00	0	0	0	6.46	7.68	0	6.44	0	7.78	12.22	4.56	4.33	78.13	0	21.86
	CMK-25	21.67	16.29	3.13	8.10	0.87	0	1.72	0	6.68	7.22	4.44	3.32	0	8.12	12.33	3.77	3.21	75.89	2.65	21.44
	TZM-24	21.58	16.22	4.12	8.55	0.00	0	1.80	0	6.32	4.21	4.45	7.28	0	6.56	12.32	3.10	3.49	80.36	2.86	16.76
	TZM-26	16.76	14.55	6.88	9.37	1.59	0	1.22	0	6.04	9.15	3.75	4.45	0	6.05	14.56	3.90	3.32	74.34	1.90	23.74
	TZM-27	17.89	15.67	5.67	8.94	0.00	0	0.69	0	4.32	9.22	2.89	5.66	0	7.90	13.89	3.89	3.37	77.19	1.10	21.69
Lower Baraill sandstones	TMK-12	23.32	17.76	6.13	10.87	0.53	0.89	0.56	0	4.20	2.65	0	6.24	3.76	8.20	10.44	2.80	2.18	87.49	2.18	10.31
	TMK-14	20.39	17.82	5.56	10.21	0.89	0.76	0	0	8.24	5.85	0	6.18	0	8.61	6.44	5.79	4.15	78.42	1.10	20.47
	TMK-15	24.12	18.68	3.70	4.98	0.00	0	0	0	7.02	4.22	0	11.62	0	7.88	11.32	3.78	2.68	82.07	0	17.92
	CMK-12	17.39	17.39	8.6	13.90	0.00	0	1.26	0	3.86	4.65	0	6.60	0	10.65	8.03	3.47	4.20	85.428	1.87	12.69
	CMK-15	18.76	20.20	8.40	12.10	0.38	0	0.80	0	3.45	5.23	0	4.50	0	8.60	11.10	2.50	4.3	86.24	1.16	12.59
	CMK-19	22.87	18.58	8.89	11.68	0.00	0	0	0	4.89	6.41	0	5.56	0	8.64	8.26	1.20	3.02	84.58	0	15.41
	TZM-01(A)	20.15	15.26	4.22	8.72	0.00	0	2.39	0	7.89	4.24	8.76	5.36	0	8.22	9.78	3.78	1.23	76.90	3.80	19.29
	TZM-08	20.07	18.15	4.16	9.93	0.00	0	2.79	0	6.00	5.49	8.69	4.97	0	4.58	9.94	2.02	3.21	78.55	4.18	17.25
	TZM-12	20.37	18.79	5.66	10.20	0.62	0	0.69	0	5.59	6.32	6.98	3.32	0	6.32	10.54	2.57	2.65	81.36	1.02	17.61
	TZM-14	18.20	18.78	4.22	7.82	0.45	0	1.68	0	5.66	7.77	4.43	4.89	0	8.91	11.53	3.23	2.88	76.43	2.61	20.94

Q_{Mu}, Monocrystalline undulatory quartz; Q_{Mnu}, Monocrystalline non-undulatory quartz; Q_{P2-3}, Polycrystalline quartz with 2–3 grains per quartz; $Q_{P>3}$, Polycrystalline quartz with >3 grains per quartz; Q_O, Quartz over growth; $P_{Ca/Na}$, Plagioclase; F_K, Potash feldspar; RF_{Ig}, Igneous rock fragment; RF_{Sed}, Sedimentary rock fragment; RF_{Met}, Metamorphic rock fragment; C_{Sil}, Siliceous cement; C_{cl}, Clay cement; C_{Fer}, Ferruginous cement; C_{Cal}, Carbonaceous/calcite cement.

under anoxic condition. They inhibit quartz cementation, but infill pore spaces[4]. The clay minerals recorded as pore lining and pore-filling cements are considered as one of the main factors for reduction of porosity in the studied sandstones. However, in the sandstones of lower Barail Group, grain coatings restrict or hinder cementation and preserve porosity during deep burial, but decrease permeability at pore throats. In certain samples, calcite cement tends to corrode the grain margins, producing irregular-shaped grains (Figure 2 *f*) and tends to suppress quartz overgrowth, thereby preserving porosity. The study shows that clay is the first-generation cement followed by ferruginous, silica and carbonate cements in the studied sandstones. The volumetric percentage of cement ranges from 12.43 to 22.34. Albitization of feldspar is a special process that involves replacement of detrital K-feldspar by albite (Figure 2 *g*)[5]. This alteration occurs along weak planes, i.e. fracture planes and cleavages, along which fluids enriched in Na^+ can penetrate the crystal. These penetrated fluids partially dissolve the K-feldspar and re-precipitated as albite. Further migration of fluids tends to promote cementation and as a result, its secondary porosity gets reduced. During this process, texture and composition of the rocks are altered. Recrystallization of clay

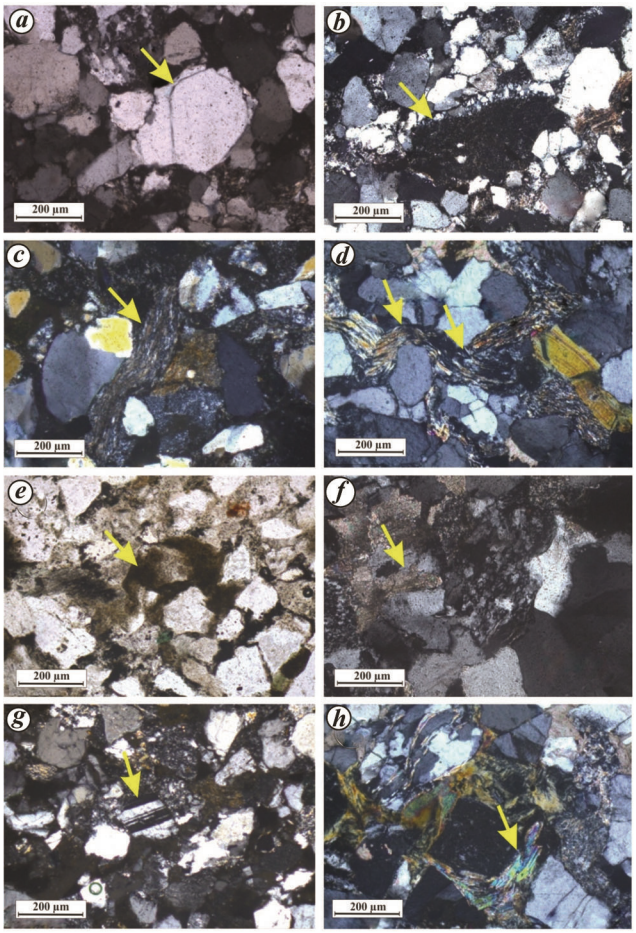

Figure 2. Photomicrographs of Barail sandstones: ***a***, Silica cement deposited as an overgrowth on detrital quartz grains. ***b***, Pseudo matrix formed from sedimentary rock fragments due to compaction. ***c***, Plastic deformation of metamorphic lithic fragments. ***d***, Kink mica showing the effect of mechanical compaction. ***e***, Iron-oxide cement occurring as scattered aggregates and pervasive pore fillings as well as a dark black coating on the detrital quartz and feldspar grains. ***f***, Calcite cement corrodes the grain margins to produce irregular-shaped grains and tends to suppress quartz overgrowth. ***g***, Replacement of weak detrital K-feldspar by albite (albitization). ***h***, Recrystallization of clay minerals to muscovite (muscovitization) under deep burial compaction indicating late stage of diagenesis.

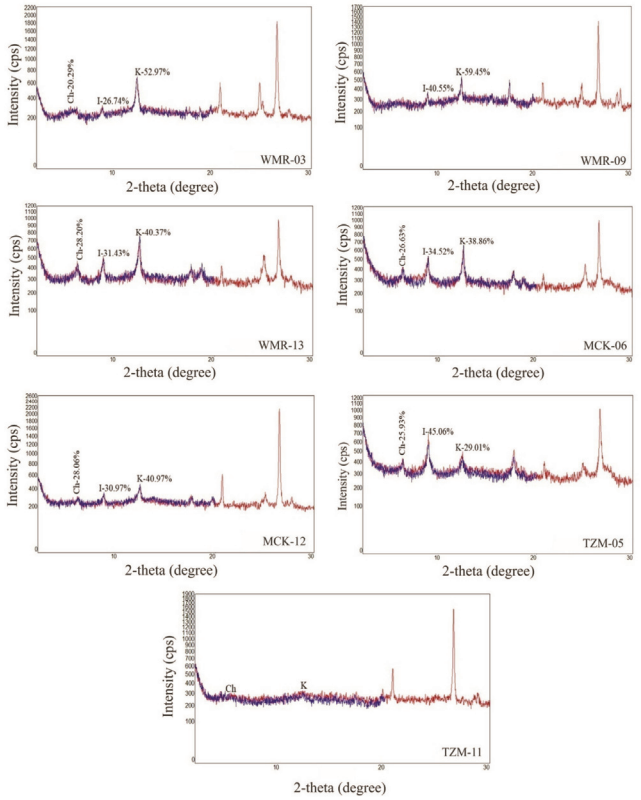

Figure 3. X-ray diffractograms of clay minerals: oriented slide (red) and glycolated slide (blue). Ch, Chlorite, I, Illite and K, Kaolinite.

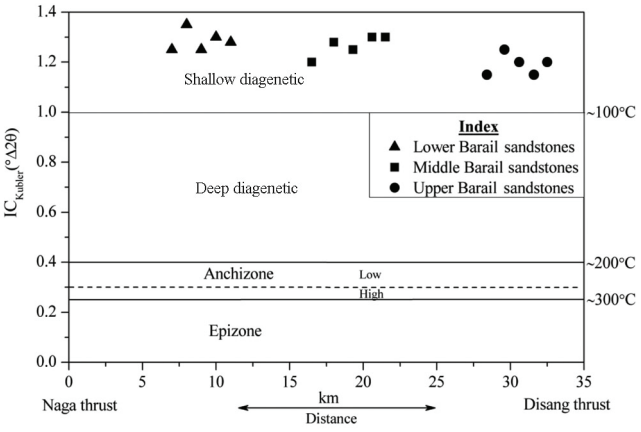

Figure 4. Plot of illite crystallinity index versus distance between the Naga thrust and Disang thrust of the study area (after Verdel *et al.*[6]).

Table 2. Laboratory-measured porosity values of Barail sandstones

Litho-unit	Sample ID	Porosity values (%)	
		Helium porosimeter	Petrographic study
Upper Barail sandstone	TMK-24	12.83	10.52
	TMK-26	10.4	7.77
	CMK-39	11.2	8.82
	CMK-41	13.08	11.22
	TZM-29	11.34	7.89
Middle Barail sandstone	TMK-16	13.68	12.12
	CMK-21	14.2	11.85
	CMK-23	13.89	12.00
	TZM-18	13.73	11.81
	TZM-23	14.32	11.53
Lower Barail sandstone	TMK-07	14.5	14.44
	TMK-12	15.19	15.58
	CMK-12	16.65	17.00
	TZM-01(A)	14.92	14.4
	TZM-08	15.48	16.66

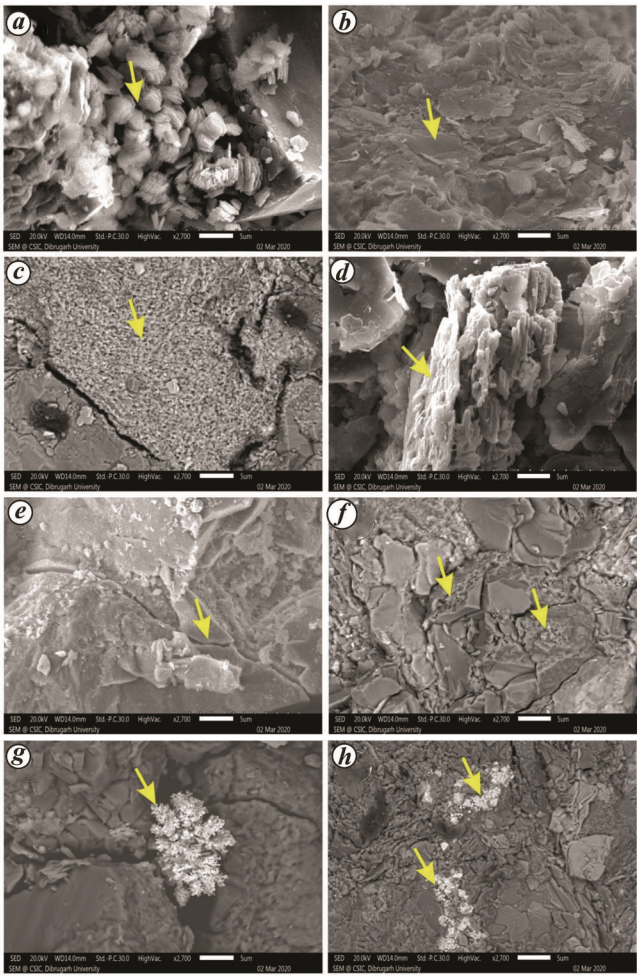

Figure 5. SEM images of Barail sandstones. ***a***, Kaolinite occurs as booklet-like and vermicular stacked crystals in the pore spaces. ***b***, Illite occurs as discontinuous platelet-like crystals. ***c***, Mixed illite–smectite layer occurs as grain-coating clay. ***d***, Recrystallization of fine matrix and dissolution of K-feldspar. ***e***, Intragranular fractures develop due to tectonic compression. ***f***, Dissolution effect on quartz. ***g***, Cluster of star-shaped cristobalite plugging the pore space. ***h***, Authigenic growth of framboidal pyrites.

minerals to muscovite under deep burial compaction indicates late stage of diagenesis (Figure 2 *h*). Such recrystallization tends to increase grain size and thereby negatively affects both porosity and permeability. X-ray diffraction (XRD) analysis shows the presence of kaolinite (avg. 49.12%), illite (avg. 36.24%) and chlorite (avg. 18.10%) in the studied sandstones (Figure 3). Kaolinite is the common authigenic clay mineral, followed by illite and mixed illite–smectite. Abundance of illite makes it possible to measure the thermal maturity of organically rich shale. The thermal maturity can be determined by measuring the illite crystallinity (IC) index, which is the full width at half maximum for the XRD peak along the basal (001) crystallographic axis of illite. IC index >1°$\Delta 2\theta$ corresponds to a metamorphic shallow diagenetic zone with temperature less than 100°C. In the studied shale samples the IC index ranged from 1.15 to 1.35°$\Delta 2\theta$ (Table 3), indicating a metamorphic shallow diagenetic zone (Figure 4)[6]. It infers a low thermal maturity for the Barail carbonaceous shale and as such they are in the initial phase of oil-generating stage. The temperature values suggest the immature or initial stage of generation of hydrocarbons from the intervening Barail carbonaceous shale. In scanning electron microscope (SEM) studies, kaolinites are recorded as patches composed of booklet-like and vermicular stacked crystals (Figure 5 *a*), and fill both the primary and secondary pores reducing the total porosity of the sandstones. Illite occurs as discontinuous platelet-like crystals (Figure 5 *b*). Mixed illite–smectite layer occurs as a grain-coating clay (Figure 5 *c*). All these clay minerals are formed due to recrystallization of fine matrix and dissolution of K-feldspar (Figure 5 *d*). Furthermore, they have been formed because of alteration of one kind of clay mineral to another. Illite changes to sericite, which later recrystallizes into muscovite[7]. Grain fracturing takes place mostly during late stage of diagenesis due to tectonic compression. As the overburden pressure

Table 3. Semi-quantitative results of X-ray diffraction analysis and illite crystallinity (IC) index

Litho-unit	Sample ID	Clay (%)			IC index (°Δ2θ)	Metamorphic zone[6]
		Kaolinite (K)	Chlorite (Ch)	Illite (I)		
Upper Barail sandstone	TMK-24	52.97	20.29	26.74	1.2	Shallow diagenetic
	TMK-26	40.37	28.20	31.43	1.2	Shallow diagenetic
	CMK-29	41.66	17.72	40.62	1.2	Shallow diagenetic
	TZM-28	44.87	8.97	46.16	1.15	Shallow diagenetic
	TZM-31	52.63	21.06	26.31	1.25	Shallow diagenetic
Middle Barail sandstone	TMK-19	59.45	–	40.55	1.25	Shallow diagenetic
	TMK-20	38.86	26.63	34.52	1.3	Shallow diagenetic
	CMK-21	22.77	9.1	67.32	1.28	Shallow diagenetic
	CMK-25	28.31	18.86	52.83	1.3	Shallow diagenetic
	TZM-23	50.04	16.33	33.33	1.15	Shallow diagenetic
Lower Barail sandstone	TMK-09	29.01	25.93	45.06	1.25	Shallow diagenetic
	TMK-11	40.97	28.06	30.97	1.3	Shallow diagenetic
	CMK-14	58.82	–	41.18	1.25	Shallow diagenetic
	CMK-19	36.77	10.29	52.94	1.28	Shallow diagenetic
	TZM-08	56	16	28	1.35	Shallow diagenetic

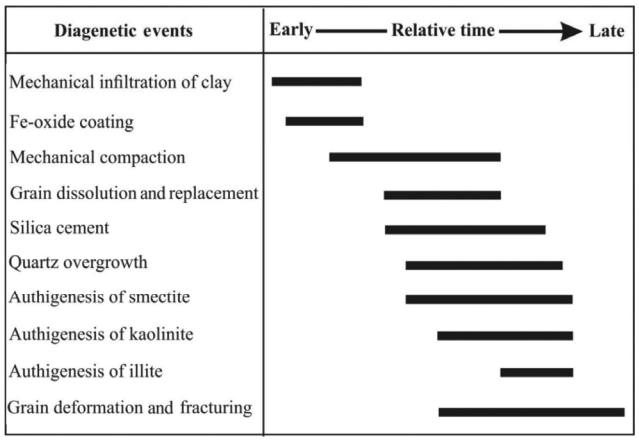

Figure 6. Summary of diagenetic events of the Barail sandstones.

and tectonic compression processes continue to occur, the rigid grains start to develop intragranular fractures (Figure 5 *e*). These fractures are influenced by the process of dissolution, which increases the secondary porosity of the rocks. The long-axis grain contacts are mostly representative of intermediate burial depth, while the concavo-convex and sutured contacts are representative of intense compaction under deep burial depth. It has been documented that finer the grain size, greater is the surface area for diagenetic alterations[8]. The Barail sandstones of the present study are mainly fine- to medium-grained. So, these sandstones have undergone all the diagenetic phases. Though dissolution on quartz and feldspars created secondary porosities in the sandstones (Figure 5 *f*), these secondary porosities were again partially filled up by cement on many occasions. The original pore morphologies as well as the secondary porosities within the sandstones tend to be destroyed to a large extent by both cementation and authigenic mineral growth (Figure 5 *g* and *h*). Therefore, the total porosity has been reduced to 7.77% in certain samples (Table 2). The porosity values of 15 core plug samples of size diameter 1.5 inch were measured (TPI-219 Helium Porosimeter, Coretest systems) at the Department of Petroleum Technology, Dibrugarh University. The ideal gas, helium (He) was used and the experiments were conducted at room temperature. The thin sections were prepared by epoxy impregnation, which gives a blue colour for the pore spaces. The coloured images of thin sections were converted to binary images (B&W), where the black colour (grains) represents '0' and white colour (pores) represents '1'. Now taking an average over the binary images gives the porosity[9]. Based on overall physical and chemical changes, a diagenetic sequence of the Barail sandstones was derived (Figure 6). The diagenetic study reveals that infiltration of clay was the first-generation cementing phenomenon; this was followed by precipitation of ferruginous cement under reducing depositional environment. As the depth of burial increased compaction of the framework grains progressively increased and loss of porosity was initiated at an early stage of burial. At intermediate to greater depth, due to increased overburden pressure the long and straight grain contacts were converted into concavo-convex and sutured contacts. As a result, silica solutions were released from the zones of the sutured contact and they percolated through the available pore spaces of coarse-grained clean sandstone. These silica solutions precipitated over the quartz grains as overgrowths reducing the primary porosity. Quartz overgrowths are common in coarse-grained clean sandstone because its high permeability permits easy percolation of water and silica-rich fluids. However, during this intermediate phase of diagenesis, the partial dissolution on quartz and feldspar grains and replacement by calcite cement were found effective. Grain dissolution associated with peripheral corrosion on framework grains preserves secondary

porosity. Precipitation of authigenic illite and mixed layer clay post-dates kaolinite and quartz overgrowths. These clay minerals reduce porosity and permeability by occurring as rims around detrital grains. Occurrence of bent mica and intragranular fractures on rigid framework grains indicates the effect of overburden pressure and tectonic compression at late stage of diagenesis.

Overall, the present study reveals the presence of both primary and secondary porosities in the sandstones. The primary porosity is mostly intergranular porosity. Secondary porosity is created by the dissolution of feldspars, quartz and other unstable minerals, and fracturing of comparatively rigid gains. However, the total porosity is destroyed to a large extent by both cementation and authigenic mineral growth. Occurrence of pyrite framboids suggests introduction of ferruginous solution at an early stage of diagenesis under anoxic condition. Oxidation of iron is superposed at a later stage. Coal seams and carbonaceous shales observed during field mapping in the upper part of the Barail Group suggest that these sediments were deposited in a lower delta plain environment. In such depositional setting, the sediments are influenced by tides as well as fluvial activities, and as a result they exhibit poorly sorted texture. So, the bottom and middle parts of the Barail sandstones show well-sorted texture and preserve higher porosity during burial, while sandstones of the upper part are poorly sorted and show low porosity. The sandstones are mostly angular to sub-angular in shape; therefore, they preserve good primary porosity. Secondary porosity is developed significantly in certain samples. The original pore morphology, as well as secondary porosity within the sandstones tends to be destroyed to a large extent by the diagenetic processes.

1. Kent, W. N. *et al.*, Application of a ramp/flat fault model to interpretation of the Naga thrust and possible implications for petroleum exploration along the Naga thrust front. *AAPG Bull.*, 2002, **86**(12), 2023–2045; https://doi.org/10.1306/61EEDDF0-173E-11D7-8645-000102C1865D.
2. Al-Gailani, M. B., Authigenic mineralizations at unconformities: implication for reservoir characteristics. *Sediment. Geol.*, 1981, **29**(2), 89–115; https://doi.org/10.1016/0037-0738(81)90001-4.
3. Folk, R. L., *Petrology of Sedimentary Rocks*, Hemphill Publ. Co., Austin, USA, 1980, p. 182.
4. Ali, A. M. *et al.*, Petrographic and microtextural analyses of miocene sandstones of onshore West Baram Delta Province, Sarawak Basin: implications for porosity and reservoir rock quality. *Petrol. Coal*, 2016, **58**(2), 162–184.
5. Aagaard, P. *et al.*, Diagenetic albitization of detrital K-feldspar in Jurassic, Lower Cretaceous and Tertiary clastic reservoir rocks from offshore Norway, II. Formation water chemistry and kinetic considerations. *J. Sediment. Petrol.*, 1990, **60**, 575–581.
6. Verdel, C. *et al.*, Variation of illite/muscovite $^{40}Ar/^{39}Ar$ age spectra during progressive low-grade metamorphism: an example from the US Cordillera. *Contrib. Mineral. Petrol.*, 2012, **164**, 521–536; https://doi.org/10.1007/s00410-012-0751-7.
7. Chima, P. *et al.*, Diagenesis and rock properties of sandstones from the Stormberg Group, Karoo Supergroup in the Eastern Cape Province of South Africa. *Open Geosci.*, 2018, **10**(1), 740–771; https://doi.org/10.1515/geo-2018-0059.
8. Baiyegunhi, C. *et al.*, Diagenesis and reservoir properties of the Permian Ecca Group sandstones and Mudrocks in the Eastern Cape Province, South Africa. *Minerals*, 2017, **7**(6), 1–26; https://doi.org/10.3390/min7060088.
9. Richa, *et al.*, Image analysis and pattern recognition for porosity estimation from thin sections. SEG Technical Program Expanded Abstracts, 2006, pp. 1968–1972; https://doi.org/10.1190/1.2369918.

ACKNOWLEDGEMENTS. We thank the Department of Petroleum Technology, Dibrugarh University for providing laboratory facilities for this study. Views expressed in this communication are those of the authors' alone.

Received 19 May 2021; revised accepted 7 September 2021

doi: 10.18520/cs/v121/i8/1107-1113

Encounter rates and density of medium and large-sized mammals with nocturnal habits in southern Amazon, Brazil

Ednaldo Cândido Rocha[1,*], Camilla Angélica de Lima[2], Nayara Lima Batista[2] and André Luís da Silva Castro[2]

[1]Universidade Estadual de Goiás, Câmpus Ipameri, Goiás, Brasil
[2]Instituto Federal Goiano, Campus Urutaí, Programa de Pós-Graduação em Conservação de Recursos Naturais do Cerrado, Urutaí, Goiás, Brasil

The aim of the present study is to calculate the encounter rate and estimate the density of medium and large-sized mammals with nocturnal habits in the Cristalino region of northern Mato Grosso, southern Amazon, Brazil, using distance sampling method. Eight species were detected with encounter rate varying from 0.09 at 1.68 encounters 10 km^{-1}, and three population densities were estimated: *Cuniculus paca* (7.75 individuals km^{-2}), *Potos flavus* (7.08 individuals km^{-2}) and *Mazama americana* (4.23 individuals km^{-2}). Our data help expand the information about density of nocturnal mammals in the southern Amazon region, in the transition between the Amazon and the Cerrado biomes, and can contribute to management and conservation of these species.

Keywords: Distance sampling, encounter rates, nocturnal mammals, population density, species abundance.

*For correspondence. (e-mail: ednaldorocha@yahoo.com.br)